Physics and Imaging in Radiation Oncology 31 (2024) 100601

Contents lists available at ScienceDirect

Physics and Imaging in Radiation Oncology

journal homepage: www.sciencedirect.com/journal/physics-and-imaging-in-radiation-oncology

Review Article

Data-driven gated positron emission tomography/computed tomography for radiotherapy

Tinsu Pan [a,*], Dershan Luo [b]

[a] Department of Imaging Physics, M.D. Anderson Cancer Center, University of Texas, United States
[b] Department of Radiation Physics, M.D. Anderson Cancer Center, University of Texas, United States

ARTICLE INFO

Keywords:
Tumor motion
Misregistration correction
Respiratory motion
Respiratory gating
PET/CT
Data-driven gated PET
Data-driven gated CT
Data-driven gated PET/CT

ABSTRACT

Purpose: Software-based data-driven gated (DDG) positron emission tomography/computed tomography (PET/CT) has replaced hardware-based 4D PET/CT. The purpose of this article was to review DDG PET/CT, which could improve the accuracy of treatment response assessment, tumor motion evaluation, and target tumor contouring with whole-body (WB) PET/CT for radiotherapy (RT).
Material and methods: This review covered the topics of 4D PET/CT with hardware gating, advancements in PET instrumentation, DDG PET, DDG CT, and DDG PET/CT based on a systematic literature review. It included a discussion of the large axial field-of-view (AFOV) PET detector and a review of the clinical results of DDG PET and DDG PET/CT.
Results: DDG PET matched or outperformed 4D PET with hardware gating. DDG CT was more compatible with DDG PET than 4D CT, which required hardware gating. DDG CT could replace 4D CT for RT. DDG PET and DDG CT for DDG PET/CT can be incorporated in a WB PET/CT of less than 15 min scan time on a PET/CT scanner of at least 25 cm AFOV PET detector.
Conclusions: DDG PET/CT could correct the misregistration and tumor motion artifacts in a WB PET/CT and provide the quantitative PET and tumor motion information of a registered PET/CT for RT.

1. Introduction

Whole-body (WB) positron emission tomography/computed tomography (PET/CT) is a comprehensive technology for structural, functional, and molecular phenotyping of cancer at the WB level. It is a standard imaging tool for managing cancer patients for surgery, radiotherapy (RT), chemotherapy, or a combination of these treatments [1]. The most used radiotracer is ^{18}F-Fluorodeoxyglucose (^{18}F-FDG), a marker for neoplastic cells' glucose avidity [2]. WB PET/CT changed patient management in more than 30 % of all cancer patients and distinguished between neoplastic and normal tissues more accurately than CT or magnetic resonance imaging [1,3,4].

Unlike CT data, which are normally acquired over a single organ at breath hold (BH), WB PET/CT data is normally taken at free breathing (FB) due to the limited geometric sensitivity of the PET scanner, which requires minutes of data acquisition, and the suggestion of maintaining a similar breathing condition for PET and CT [5]. Effective mitigation of image blurring caused by respiratory motion is critical to preserve 3–5 mm PET spatial resolution [6]. The other degradation by respiratory motion is misregistration between PET and CT [7]. Issues related to misregistration between slow PET and fast CT, and motion blur in PET images have been actively researched since the first commercial PET/CT in 2000 [8].

Misregistration could mistake a true positive for a false negative response [9]. It could also induce artifactual myocardial defects in 40 % of cardiac PET/CT imaging [10]. Using average CT over one respiratory cycle is an effective solution to improve the registration of CT and PET [11]. However, average CT may not register well with gated PET and was shown to be negatively impacted by irregular respiration [12]. BH at normal expiration during CT acquisition could improve the registration between CT and PET [13]. However, this typically requires coaching the patient to BH with a respiratory monitoring device (RMD), which is inconvenient to perform in a clinical setting [14].

The extent of PET quantitation errors in the region of misregistration depends on the degree of misregistration between PET and CT and the distribution of radiotracer surrounding the misregistration area [15].

* Corresponding author at: Department of Imaging Physics, UT MD Anderson Cancer Center, Houston, 1515 Holcombe Blvd. Unit 1352, Houston, TX 77030-4009, United States.
E-mail address: tpan@mdanderson.org (T. Pan).

https://doi.org/10.1016/j.phro.2024.100601
Received 7 April 2023; Received in revised form 17 June 2024; Accepted 18 June 2024
Available online 26 June 2024

Without any correction of respiratory motion or misregistration artifacts, clinical trials of patients with advanced non-small cell lung cancer suggested that for lesions greater than 2 cm in size and with maximum standardized uptake value (SUV_{max}) greater than 4.0, changes in tumor ^{18}F-FDG uptake had to be more than 40 % to reflect metabolic response or metabolic progression [16]. This 40 % uncertainty could be potentially reduced by the corrections of tumor motion and misregistration artifacts.

4D CT and 4D PET/CT (attenuation correction of 4D PET by 4D CT) were proposed as a solution to manage the issues related to respiratory motion in FB CT and FB PET/CT imaging, respectively [17,18]. 4D CT is designed to image tumor motion in RT, while 4D PET/CT is to mitigate the impact of tumor motion and to improve the quantification of radiotracer uptake in PET [17,18]. 4D CT can be performed with a cine CT or a low-pitch helical CT and has become a standard imaging procedure for RT [19,20]. 4D PET/CT, on the other hand, has not been widely utilized due to its requirement of both 4D PET and 4D CT, complexity in implementation, and limited studies to suggest its clinical utility [16,21–23].

4D CT and 4D PET/CT studies rely on a respiratory monitoring device (RMD) or surface tracking [18,19,24]. An RT session 4D CT normally lasts around 30–45 min, with most of the time devoted to patient setup and immobilization [25]. A 4D PET/CT imaging may exceed 60 min on a PET/CT scanner with a 15-cm axial field of view (AFOV) detector [18]. Active patient collaboration in maintaining regular and reproducible breathing is essential for the quality of 4D CT and 4D PET/CT [26].

About 50 % of cancer patients receive RT during treatment [27]. Application of 4D PET/CT in RT is limited because patients typically receive their PET/CT scans for diagnostic imaging before they become candidates for RT, making additional PET/CT for RT unlikely. Additionally, most PET/CT scanners are at facilities dedicated to diagnostic imaging, where patient throughput is critical. It will be desirable to make every WB PET/CT free of misregistration and motion artifacts without an RMD to benefit RT [12,28–31]. The purpose of this article was to review DDG PET/CT, which could improve the accuracy of treatment response assessment, and supplement 4D CT or potentially replace 4D CT for the management of tumor motion in RT.

2. Material and methods

This review focused on DDG PET/CT advancements. The topics covered were state-of-the-art PET/CT, DDG PET, DDG CT, and DDG PET/CT. It included a discussion of the large AFOV PET detector and a review of the clinical results of DDG PET and DDG PET/CT. A search of PUBMED with the keywords ‘device-less PET’, ‘device-less CT’, ‘data-driven gated CT’, ‘data-driven gated PET’, ‘data-driven CT’, ‘data-driven PET’, ‘software gating’, ‘motion correction’, ‘motion estimation’, and ‘respiratory gating’, on May 1, 2024, resulted in 80 articles excluding the articles for head motion or unrelated to PET. These articles were included in the review. Topics of PET/CT motion management for RT and respiratory gating of PET have been reviewed elsewhere [23,26,32].

3. Results

3.1. State of the art PET/CT

Modern PET/CT scanners were equipped with (1) 3D scanning to improve geometric sensitivity (cps/kBq, counts detected per second per kilo Becquerel of radioactive activity) [33]; (2) time-of-flight (TOF) to improve localization accuracy of the detected coincidence events in image reconstruction [34]; (3) silicon photomultiplier (SiPM) to improve the accuracy of position detection of the detected 511 keV photons [35]; (4) a large AFOV detector of at least 25 cm to improve geometric sensitivity [36–38]; and (5) DDG PET to enable respiratory gating for every PET scan without the hardware gating with an RMD or surface tracking [30,39].

For CT registration with DDG PET, all commercial systems required 4D CT, which needs hardware gating with an RMD or surface tracking [19,20]. This combination of 4D CT and DDG PET made patient preparation and scanning challenging and motivated the development of a new DDG CT [12,31].

3.2. Data-driven gated PET

DDG PET, which gates PET data based on a respiratory signal extracted from a series of dynamic PET data of either image, sinogram, or list mode data was a promising technique for improving PET quantification. It normally required noise reduction and a strategy of retaining the dominant breathing frequency of a respiratory signal. For automation, the periodicity of respiratory motion was measured as a parameter for the initiation of DDG PET. In addition to coincidence events, singles were also used for fast respiratory motion detection [40].

3.2.1. Center of mass (CM)

The technique was first proposed to detect respiratory motion in list mode PET data where the contrast of tracer to background is high [41]. The axial or superior–inferior component of the sinogram CM of the radiotracer every 0.5 s was calculated to serve as an indicator of motion. This method did not require the reconstruction of images and could be applied to motion detection at a fine temporal scale. The radiotracer distribution should remain fairly constant throughout the PET acquisition [41]. A respiratory signal was also derived by analyzing the CM of a region of interest (ROI) in dynamic PET images or following the CM in a targeted tumor [42–44]. TOF information could be incorporated to reduce contributions from the stationary background and to improve the CM calculation [45].

For the derivation of a respiratory signal, the ROI was extended to an entire AFOV for the total counts based on the property of geometric sensitivity, highest in the middle and lowest at the edge of the AFOV [46]. Respiratory motions in the superior-inferior and anterior-posterior directions were determined by computing the centroid of distribution (COD) of all coincidence events during each short time frame. Activity in and out of the AFOV introduced some uncertainty to this method [46,47]. The approach could also be enhanced by TOF information [48].

An adaptive CM approach of incorporating TOF information was proposed for automatic ROI selection to produce a prominent respiratory signal in the axial direction [28]. This approach calculated the centroid of an ROI that only contains regions with a large motion or a high tracer uptake and avoided manual selection of an ROI. It obtained the respiratory signal with the highest signal prominence, a ratio of the mean energy of the signal inside a respiratory frequency range to the mean energy of the noise outside the respiratory frequency range, over many ROIs [49]. This approach was not effective if there was a limited radiotracer uptake in the AFOV and could be improved with a larger AFOV detector to cover a larger anatomy with more radiotracer uptake [28].

3.2.2. Time-activity curves (TAC)

Respiratory motion was estimated by the time-activity curves (TAC) of the ROIs at the interface of the lungs with the chest walls or the diaphragm in dynamic PET images [50]. This was achieved by placing an ROI in such a way that the organ of interest was inside the ROI during a part of the motion cycle, while during the other part of the cycle, it was outside. This ensured that the maximum amount of signal was captured, and the resulting TAC was accurate. The frequency of respiration was estimated by the Fourier transform of the respiratory signal [50].

A fully automated method based on the TAC of each voxel in the image data was also proposed [51]. Five hundred voxels with the highest cranial-caudal activity gradient (difference between adjacent voxels along the axial direction), normally at the edges of the radiotracer activity in the images, were selected to cumulatively “grow” or combine the TAC at many voxels into a global respiratory signal over 500 iterations. A quality factor was introduced to suggest confidence in the respiratory signal for gating [51,52]. To avoid lengthy image reconstruction time, this approach was later applied to the TAC of ROIs in sinogram data [39].

3.2.3. Spectral analysis

In spectral analysis, the sinogram data were smoothed, Fourier transformed to the power spectrum and threshold at each pixel location with a spectral window for identification of a potential frequency of respiration [29]. This calculation was applied to all angles of the sinogram data to determine the most dominant frequency component of respiration. Pixels whose frequency values were close to the most dominant frequency were used to define a binary mask to eliminate the pixels that were not subject to respiratory motion. The total counts within the regions in the mask varied proportionally with the displacement of an edge moving within the mask. This approach was extended from sinogram to image space, where the TOF information was used to backproject coincidence events into their most probable voxels. Similar to the sinogram approach of the same method, it also masked and removed voxels not affected by the respiratory motion [53]. This approach has also been extended to PET/CT scanners of continuous bed motion, whose patient table position changed continuously during data acquisition [53].

3.2.4. Principal components analysis (PCA)

This approach calculated the weighting factors of the first three principal components in the sinogram over time, and the weighting factors were Fourier transformed for the peak frequency value within the 0.1–0.4 Hz range, corresponding to a breathing cycle of 2.5–10 s. The respiratory signal in the frequency domain was converted to the time domain. A peak detection algorithm was applied to derive the end-inspiration (EI) phases for gating. The ratio of the peak frequency value within 0.1–0.4 Hz to the mean frequency value outside 0.1–0.4 Hz was defined as the strength of the respiratory signal. Respiratory gating was activated prospectively once the ratio exceeded a set threshold during data acquisition or activated retrospectively after data acquisition [30]. This approach was validated with hardware gating [54]. PCA was less impacted by noisy data than spectral analysis or COD [55]. PCA also had a higher correlation with external gated signals than COD [56].

Principal components are a linear combination of the original variables that maximally explain the variance of all the variables. PCA sorted the data variance into major features on the leading dimensions and random noise on the minor dimensions [57]. To extract useful features from a non-linear space, an unsupervised deep-learning clustering network was proposed that employed an autoencoder to extract latent features from short-time frame images without attenuation, scatter, or randoms corrections, followed by K-means clustering of the latent features for respiratory gating [58].

3.2.5. Phase determination in DDG PET

Phase determination is important when the respiratory signals from multiple bed positions of PET data are combined for the reconstruction of DDG PET also from multiple bed positions to register with CT data. Many methods provided signals whose direction related to the physical motion was uncertain, i.e., their sign was arbitrary, therefore a maximum in the signal could refer to either EI or end-expiration (EE) phase, which could cause inaccurate motion correction [59].

As most internal organs move in the superior-inferior direction during respiration, the sagittal and coronal maximum intensity projection (MIP) images of the gated reconstructions were reduced in dimension and registered in 1-D. The respiratory phases were represented by the temporal changes or displacements to the averaged 1-D signal [59]. Gradients calculated in the axial direction of the sinogram represented weights in the direction of motion. An increase in the weights corresponded to motion toward the head or an expiratory phase. In contrast, a decrease corresponded to motion toward the feet or an inspiratory phase. The magnitude of weight became the amplitude of a respiratory signal [60]. Properties of expiration longer than inspiration in a respiratory cycle and a relatively consistent pattern of respiration were used to ensure the integrity of a respiratory signal in phase determination [28].

3.3. Large AFOV detector and DDG PET

The performance of DDG PET is improved by a large AFOV detector of at least 25 cm so that more data is collected in a shorter acquisition time as gating typically increases the noise of PET data.

As an example, GE Discovery MI (DMI) of AFOV = 25 cm and GE Discovery 710 (D710) of AFOV = 15 cm (GE Healthcare, Waukesha, USA) were compared in Table 1 [38]. The improvements in geometric sensitivity and TOF timing resolution for AFOV = 25 cm vs AFOV = 15 cm were 2.68 and 1.42 times, respectively [38]. Large geometric sensitivity, long scan time, and short TOF timing resolution all improved the signal-to-noise ratio (SNR) [61].

Reducing the scan time from 3 min/bed-position on D710 to 2 min/bed-position on DMI still favored DMI for SNR by 1.59 times. As a result, DMI achieved a better image quality than D710 and completed a WB PET/CT of about 100 cm in 10 min for 5 bed-positions vs 21 min for 7 bed-positions.

High geometric sensitivity opened up BH imaging on PET. A deep inspiration breath hold (DIBH) of 4 × 18 s on the Siemens Vision Quadra scanner of 104 cm AFOV was proposed for mediastinal lymphoma patients with pre-chemotherapy PET/CT to improve post-chemotherapy planning [62].

3.4. Clinical evaluations of DDG PET

DDG PET matched or outperformed 4D PET and could be more easily integrated into the clinic than 4D PET. DDG PET was comparable or preferable to 4D PET in a study of 219 scans [63]. DDG PET outperformed 4D PET in 13 % of cases while the opposite was true in only 2 %. Overall image quality of DDG PET was preferred over 4D PET and 4D PET had a higher failure rate than DDG PET in identifying the EI phases of the respiratory signal in a study of 144 patients [64]. A similar finding of comparable performance was reported in a study of 56 patients on a PET/CT scanner of continuous bed motion [53]. In a study of 200 patients, physicians preferred DDG PET over static PET and DDG PET over 4D PET [65].

Many patients are covered by a warm blanket in WB PET/CT for diagnostic imaging due to a low temperature setting in the scanner room, preventing optical surface tracking or direct contact between the patient's skin and a gating device. Placing a strain gage sensor around the patient for respiratory gating was considered "moderate" to "difficult" by the technologist in 27 % of patients and added 72 s of contact time between the patient and technologist [65]. Compared to 4D PET, DDG PET offered an improved workflow without any setup time and no additional radiation exposure to the technologist, who was required to place an RMD on the patient.

Table 1
Major performance parameters of D710 and DMIC.

	15 cm (D710)	25 cm (DMI)
Scintillator material	LYSO (PMT)	LYSO (SiPM)
Scintillator dimensions (mm^3)	4.2 × 6.3 × 25	3.95 × 5.3 × 25
Geometric Sensitivity (cps/kBq)	7.3	19.6
Slices × Thickness (mm)	47 × 3.27	89 × 2.8
Spatial resolution (mm)@1 cm	4.6	4.3
Spatial resolution @10 cm	5.1	4.9
Timing resolution (10^{-12} s)	545	385
Percent overlap between two beds	27.6 % (13 slices)	28.1 % (25 slices)
Advancement per bed (cm)	11.8	17.9

DDG PET required additional scan time to reduce noise in PET images due to gating [18]. In a study of 149 patients for cancer staging and restaging, in 85 % of the patient scans, at least one bed-position exceeded the threshold of gating and the scan time was doubled for DDG PET [66]. Overall image quality was comparable between static and DDG PET. Tumor blurring was reduced. The organ boundary of the liver or spleen became sharper with DDG PET. DDG PET also resulted in a change of report in 27 % of the cases and a change of clinical management in 8 % of the cases. Overall scan time was increased by 4.4 min per patient on the GE DMI 25-cm AFOV scanner [66].

On the other hand, in a study of 45 lung or liver lesions from 27 patients scanned for 12 min on a PET scanner of 15-cm AFOV, DDG PET of preserving 50 % data at 3 min/bed-position did not lead to inaccurate or biased SUV_{max} [67]. In another study of 40 patients who had at least one lung or liver lesion, there was no significant difference in clinical evaluation or quantification with SUV_{mean} even when the injected activity was reduced to only 25 %, suggesting DDG PET was effective even with a regular scan protocol without an increase of scan time [68]. It was possible to combine various phases of DDG PET into a single phase of DDG PET by deformable image registration (DIR) to maintain the same noise level as the static PET without an increase in scan time [69].

Mitigation of misregistration between DDG PET and WB CT was attempted by asking the patient to deep expiration breath hold (DEBH) during CT acquisition. However, there was no difference between FB CT and DEBH CT for registration with DDG PET in a study of 147 patients [70]. Two patients were coached to BH at the EE phase for CT to match successfully with the gated PET data also at the EE phase. However, this approach required a technologist to place an RMD to coach patient BH at the EE phase [14].

3.5. DDG CT

DDG CT could be derived from the cine CT data [19]. The time-summation curves of the CT numbers for self-gating were calculated in ROIs on the interfaces between the lung and the diaphragm or between the chest walls and the lungs [19]. This was similar to the use of TAC in DDG PET [50].

Alternative approaches included iteratively searching for consistent 3D volumes over the cine CT images across cine CT scan positions [71], and tracking the four features of air content, lung region, lung density, and body region in the cine CT images and selecting the features based on spatial consistency between the signals across the cine CT scan positions [72]. Adding features based on low-frequency components of the Fourier transform of the cine CT image and using a normalized cross correlation between features to select features at each CT scan position also showed promising results [73]. A normalized cross-correlation was maximized between images of adjacent and overlapped cine CT positions as part of an image-based sorting algorithm [74]. GE's D-4D used the same features of air content, lung region, lung density, and body region and modified certain parts of the process in an attempt to minimize the impact of artifacts from irregular respiration [75].

DDG CT has been developed solely on cine CT, one of the standard CT acquisition modes on the GE CT scanners. Both cine CT and low-pitch helical CT have been correlated with the breathing signal from RMD for 4D CT imaging in RT [19,20]. Unfortunately, low-pitch helical CT could not be separated from 4D CT to stand alone because its image reconstruction needs information of the EI phases of the respiratory signal [76].

A new DDG CT to realize DDG PET/CT in less than 15 min of scan time was proposed on a PET/CT scanner with a 25-cm AFOV detector [12,31]. The radiation dose of this DDG CT for a scan coverage of 15.4 cm was 1.3 mSv [31], lower than the 5 mSv reported in an earlier implementation of DDG CT [29]. This radiation dose was less than 10 % of the radiation dose for 4D CT in RT [11,19,76]. In this new DDG CT (see Fig. 1), the lung regions and the body contours were segmented to calculate lung densities and to estimate the change of the body contours, respectively [12]. The CT images with the smallest and largest lung densities were labeled the EI and EE phases, respectively. In the images

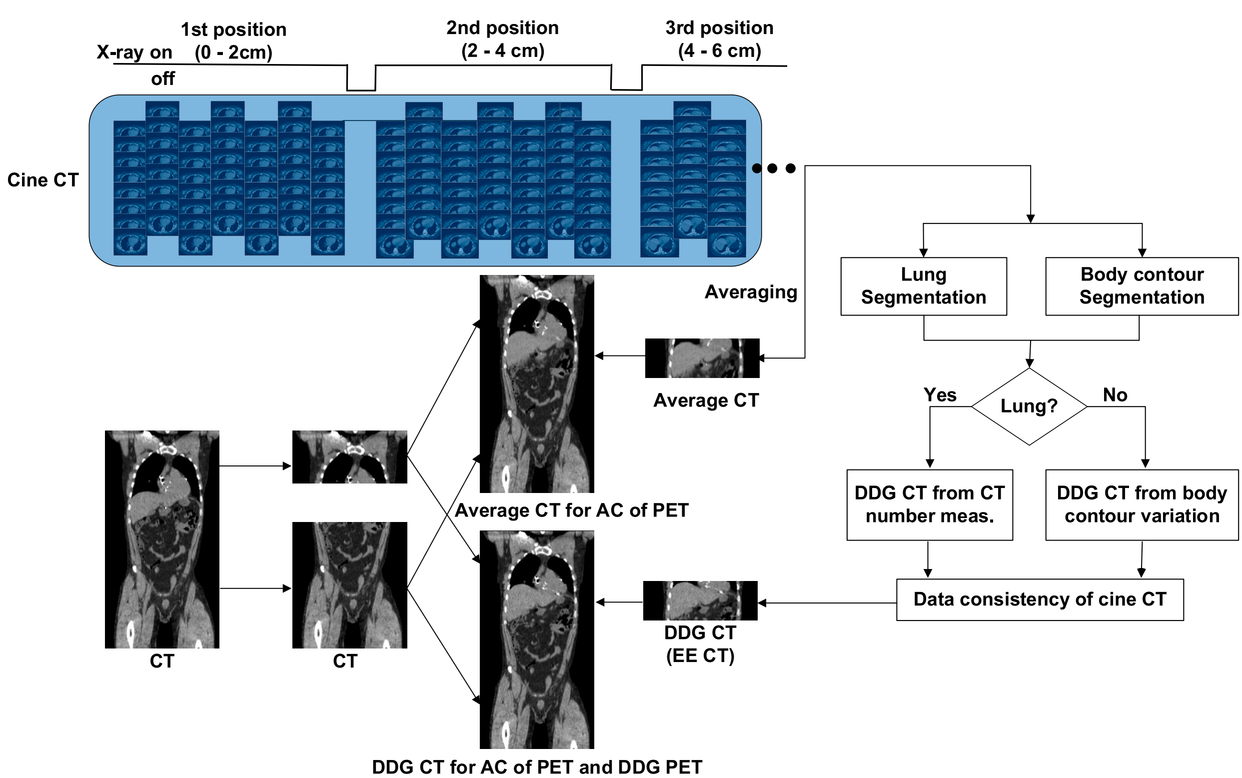

Fig. 1. Flow chart of a DDG CT. Cine CT images acquired over one breathing cycle are averaged for average CT and processed for DDG CT of EE and EI phases based on the CT numbers in the lungs and the changes in the body contours. A portion of WB CT overlapping with cine CT is replaced by average CT and DDG CT for attenuation correction of PET and DDG PET data, respectively. Inserting a small CT into WB CT makes quantification possible without a repeat of WB CT.

without the presence of a lung, the CT images at each cine position with the largest and smallest body contours were labeled the EE and EI phases, respectively. Combining a limited coverage DDG CT and a WB CT for quantification of the PET data reduced the CT radiation dose and saved the scan time for the patient because it did not require a repeat PET/CT [31].

Mitigation of irregular respiration could be performed by interactively pausing the cine CT scan when irregular respiration occurred and resuming the cine CT scan when respiration became regular [77]. A new intelligent 4D CT, also based on cine CT, was recently developed to mitigate irregular respiration prospectively for 4D CT [78]. This might suggest a transition of low-pitch helical to cine CT scans in the future.

3.6. DDG PET/CT

The first DDG PET/CT was based on spectral analysis to find regions within PET sinograms and CT images subject to respiratory motion [29]. The respiratory signals of hardware gating were also collected for 4D PET/CT to compare with DDG PET/CT. Two of the four CT datasets in this study had reduced artifacts in DDG CT than in 4D CT, suggesting that the respiratory gating was better achieved in DDG CT than in 4D CT [29].

The second DDG PET/CT study included 35 patients whose PET/CT data exhibited misregistration [31]. DDG PET/CT was better for quantification and registration of the PET/CT data than DDG PET with FB CT. Compared with repeat PET/CT, DDG PET/CT reduced CT radiation dose by 65 %, and did not need a repeat PET scan and thus reduced PET acquisition time by 6 min [31]. DDG CT also outperformed GE's D-4D CT for registration with DDG PET because the 50 % phase in D-4D, the midpoint between two EI phases of 100 %, did not possess the largest lung density as the EE phase did in DDG CT. Although D-4D CT and DDG CT were based on the same cine CT images, their registrations with DDG PET were different [12].

Two patient studies not published before were included here for an illustration of potential improvements in tumor localization and quantification by DDG PET/CT. In Fig. 2, two liver lesions correctly identified in DDG PET/CT were mistaken as one lung lesion and one heart lesion in the baseline (static) PET/CT and DDG PET (corrected by misaligned baseline FB CT). Both localization and quantification were improved by the corrections of misregistration and tumor motion in DDG PET/CT. In this example, improvements were driven mostly by misregistration correction by DDG CT rather than by tumor motion correction by DDG PET. In Fig. 3, DDG PET at EI and DDG PET at EE were attenuation-corrected by DDG CT at EI and DDG CT at EE, respectively. Improvements in image quality without tumor motion were apparent. In addition to DDG PET/CT data at the EI and EE phases, the MIP CT and average CT from the cine CT images could also be generated to support RT [19].

DDG PET/CT is a special case of DDG PET when both DDG PET and DDG CT are in the same phase. As misregistration becomes more prominent, the impact of motion correction with DDG PET is diminished. The potential benefits of DDG PET toward accurate lesion segmentation and quantitation could be fully realized when combined with DDG CT. These results impress upon the necessity of ensuring both misregistration and motion correction are accounted for together to optimize the clinical utility of PET/CT [79].

4. Discussions

One major difference between DDG PET and DDG CT is that dynamic PET data used in DDG PET can be derived from the list mode PET data, available on most PET scanners; whereas the cine CT for DDG CT is only available on the GE CT scanners [19,80]. A new prospective 4D CT, also based on cine CT, was recently commercialized [78]. It marked the change of low-pitch helical CT to cine CT scan for 4D CT by a vendor. Cine CT has the potential to become popular in the future.

DDG CT has been applied to the PET/CT data impacted by misregistration [12,31]. This requires a technologist to review PET/CT images at the last bed position of PET acquisition. If misregistration is identified, the patient is transitioned after the PET scan to the CT scan position, and a cine CT scan of about 1 min for DDG CT is taken for misregistration correction between CT and PET and to reduce tumor motion in DDG PET/CT [12,31].

If there is little tumor motion or misregistration between PET and CT, respiratory motion correction may not be necessary. This is often the case when patients are shallow breathing or when there is no tumor in the lower lungs or upper abdomen. When artifacts occur, some scans benefit from misregistration correction, motion correction, or both misregistration and motion corrections. The current solution from the vendors is DDG PET and 4D CT, which requires hardware gating, instead of DDG PET and DDG CT, which requires no hardware gating. The combination of DDG PET and DDG CT for DDG PET/CT is needed to improve the efficiency of WB PET/CT scans and fully realize the potential benefits of accurate lesion segmentation and quantitation [79].

One approach to avoid DDG CT is to find a reference PET phase to best match with FB CT and DIR the FB CT to match with PET or DDG PET

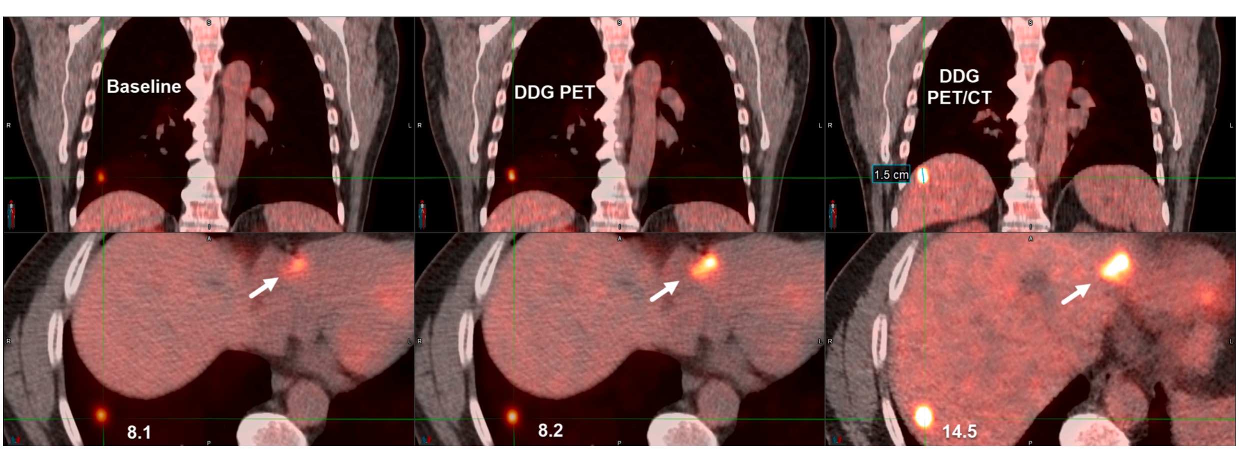

Fig. 2. From left to right are the baseline WB PET/CT, DDG PET (attenuation correction by WB CT in the baseline WB PET/CT), and DDG PET/CT (DDG PET attenuation correction by DDG CT) of an ^{18}F-FDG study. The top and bottom rows are coronal and axial fusions of the PET and CT images. A liver lesion of 1.5 cm at the cross-hair in DDG PET/CT was mispositioned to the lungs in the baseline WB PET and DDG PET. The SUV_{max} of the liver lesion was 8.1, 8.2, and 14.5 for the baseline WB PET/CT, DDG PET, and DDG PET/CT, respectively. The liver lesion by an arrow in DDG PET/CT was also mispositioned to the heart in the baseline WB PET/CT and DDG PET.

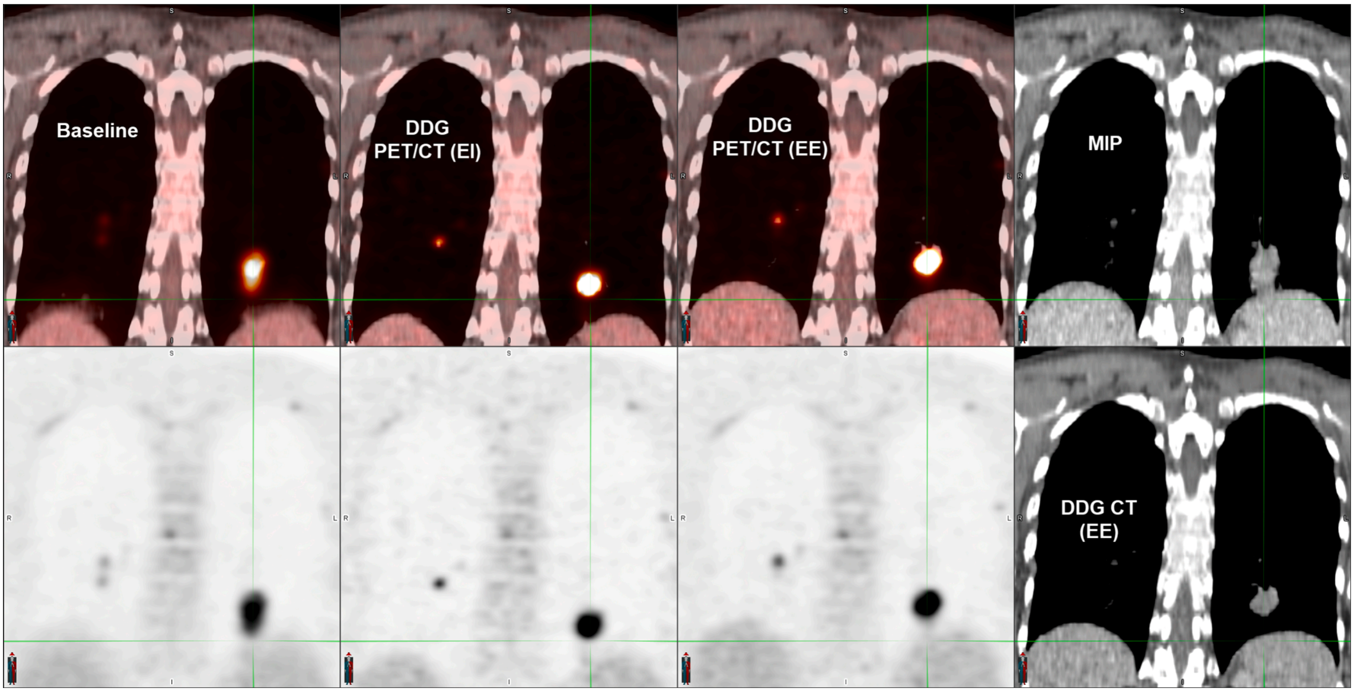

Fig. 3. DDG PET/CT for RT of an ^{18}F-FDG study. The first three columns are the baseline WB PET/CT (the top is the fusion of PET and CT, and the bottom is PET only), DDG PET/CT at EI, and DDG PET/CT at EE. The MIP CT and DDG CT at EE are in the last column. The motion blur of the two lesions in PET was mitigated in both the EI and EE DDG PET/CT.

based on the respiratory motion model derived from DDG or 4D PET [58,81,82]. However, a sigh or irregular respiration during the FB CT scan could degrade the effectiveness of DIR registration. One issue with this approach is the assumption that FB CT represents one phase of respiration. Since each CT slice captures a specific respiratory phase, the combined FB CT scan may not accurately represent any single respiratory phase [12].

Another issue is that the extent of misregistration can be up to four times the respiratory motion estimated from the EI and EE phases of DDG PET, and it can lead to distortion of the anatomy in the DIR-matched CT data [81]. FB CT can also be used to generate matched 4D CT for 4D PET based on the respiratory motion model from 4D PET [83]. Synthetic CT generated from PET without AC via machine learning is also gaining popularity for matching PET data without a real CT. TOF maximum-likelihood attenuation and activity estimation can also be used to generate an attenuation map for an improved respiratory motion model from DDG or 4D PET [84–86]. The estimated attenuation map for PET can be converted to CT images via machine learning convolution neural network [87]. However, these approaches tend to generate CT images of lower spatial resolution, and their tumor localization capabilities are still unknown. In addition, the DIR methods may not work well when FB CT does not match well with any phase of DDG or 4D PET but is still forced to match with one of the PET phases [81].

CRediT authorship contribution statement

Tinsu Pan: Conceptualization, Methodology, Software, Investigation, Data curation, Writing – original draft, Writing – review & editing. **Dershan Luo:** Investigation, Data curation, Writing – original draft, Writing – review & editing.

Declaration of competing interest

The authors declare that they have no known competing financial interests or personal relationships that could have appeared to influence the work reported in this paper.

Acknowledgements

The authors thank the reviewers for providing valuable suggestions and comments to enhance the quality of this article. The DDG PET/CT studies in this article were covered in a protocol 2021-0999 approved by the Institutional Ethics Review Board at the MD Anderson Cancer Center (MDACC). This work was supported in part by NIH R01-HL157273-01, NIH R01-EB034692-01, a ROSI grant from the Division of Radiation Oncology at MDACC, a CCSG grant from the Radiation Oncology and Cancer Imaging Program at MDACC, and a grant from the Division of Radiation Oncology and the Division of Diagnostic Imaging at MDACC.

References

[1] Czernin J, Allen-Auerbach M, Nathanson D, Herrmann K. PET/CT in oncology: current status and perspectives. Curr Radiol Rep 2013;1:177–90. https://doi.org/10.1007/s40134-013-0016-x.

[2] Pacak J, Cerny M. History of the first synthesis of 2-deoxy-2-fluoro-D-glucose the unlabeled forerunner of 2-deoxy-2-[18F]fluoro-D-glucose. Mol Imaging Biol 2002;4:352–4. https://doi.org/10.1016/s1536-1632(02)00083-5.

[3] Menon H, Guo C, Verma V, Simone 2nd CB. The role of positron emission tomography imaging in radiotherapy target delineation. PET Clin 2020;15:45–53. https://doi.org/10.1016/j.cpet.2019.08.002.

[4] Reinert CP, Sekler J, la Fougere C, Pfannenberg C, Gatidis S. Impact of PET/CT on clinical management in patients with cancer of unknown primary-a PET/CT registry study. Eur Radiol 2020;30:1325–33. https://doi.org/10.1007/s00330-019-06518-9.

[5] Bettinardi V, Picchio M, Di Muzio N, Gianolli L, Gilardi MC, Messa C. Detection and compensation of organ/lesion motion using 4D-PET/CT respiratory gated acquisition techniques. Radiother Oncol 2010;96:311–6. https://doi.org/10.1016/j.radonc.2010.07.014.

[6] Daou D. Respiratory motion handling is mandatory to accomplish the high-resolution PET destiny. Eur J Nucl Med Mol Imaging 2008;35:1961–70. https://doi.org/10.1007/s00259-008-0931-x.

[7] Lin E. Apparent posterior misregistration of a liver lesion on PET/CT: pitfall secondary to partial hepatectomy. Clin Nucl Med 2008;33:215–7. https://doi.org/10.1097/RLU.0b013e318162db5f.

[8] Townsend D, Beyer T, Czernin J. 20 years of PET/CT: a conversation with David Townsend and Thomas Beyer. J Nucl Med 2020;61:1541–3. https://doi.org/10.2967/jnumed.120.257725.

[9] Pan T, Mawlawi O. PET/CT in radiation oncology. Med Phys 2008;35:4955–66. https://doi.org/10.1118/1.2986145.

[10] Gould KL, Pan T, Loghin C, Johnson NP, Guha A, Sdringola S. Frequent diagnostic errors in cardiac PET/CT due to misregistration of CT attenuation and emission PET images: a definitive analysis of causes, consequences, and corrections. J Nucl Med 2007;48:1112–21. https://doi.org/10.2967/jnumed.107.039792.
[11] Pan T, Mawlawi O, Luo D, Liu HH, Chi PC, Mar MV, et al. Attenuation correction of PET cardiac data with low-dose average CT in PET/CT. Med Phys 2006;33:3931–8. https://doi.org/10.1118/1.2349843.
[12] Pan T, Thomas MA, Luo D. Data-driven gated CT: an automated respiratory gating method to enable data-driven gated PET/CT. Med Phys 2022;49:3597–611. https://doi.org/10.1002/mp.15620.
[13] Goerres GW, Kamel E, Heidelberg TN, Schwitter MR, Burger C, von Schulthess GK. PET-CT image co-registration in the thorax: influence of respiration. Eur J Nucl Med Mol Imaging 2002;29:351–60. https://doi.org/10.1007/s00259-001-0710-4.
[14] Daouk J, Fin L, Bailly P, Meyer ME. Improved attenuation correction via appropriate selection of respiratory-correlated PET data. Comput Methods Programs Biomed 2008;92:90–8. https://doi.org/10.1016/j.cmpb.2008.06.014.
[15] Holman BF, Cuplov V, Hutton BF, Groves AM, Thielemans K. The effect of respiratory induced density variations on non-TOF PET quantitation in the lung. Phys Med Biol 2016;61:3148–63. https://doi.org/10.1088/0031-9155/61/8/3148.
[16] Weber WA, Gatsonis CA, Mozley PD, Hanna LG, Shields AF, Aberle DR, et al. Repeatability of 18F-FDG PET/CT in advanced non-small cell lung cancer: prospective assessment in 2 multicenter trials. J Nucl Med 2015;56:1137–43. https://doi.org/10.2967/jnumed.114.147728.
[17] Vedam SS, Keall PJ, Kini VR, Mostafavi H, Shukla HP, Mohan R. Acquiring a four-dimensional computed tomography dataset using an external respiratory signal. Phys Med Biol 2003;48:45–62. https://doi.org/10.1088/0031-9155/48/1/304.
[18] Nehmeh SA, Erdi YE, Pan T, Pevsner A, Rosenzweig KE, Yorke E, et al. Four-dimensional (4D) PET/CT imaging of the thorax. Med Phys 2004;31:3179–86. https://doi.org/10.1118/1.1809778.
[19] Pan T, Lee TY, Rietzel E, Chen GT. 4D-CT imaging of a volume influenced by respiratory motion on multi-slice CT. Med Phys 2004;31:333–40. https://doi.org/10.1118/1.1639993.
[20] Keall PJ, Starkschall G, Shukla H, Forster KM, Ortiz V, Stevens CW, et al. Acquiring 4D thoracic CT scans using a multislice helical method. Phys Med Biol 2004;49:2053–67. https://doi.org/10.1088/0031-9155/49/10/015.
[21] Chi A, Nguyen NP. 4D PET/CT as a strategy to reduce respiratory motion artifacts in FDG-PET/CT. Front Oncol 2014;4:205. https://doi.org/10.3389/fonc.2014.00205.
[22] Kuykendall CC, Budzevich MM, Latifi K, Moros EG, Hoffe SE, Dilling TJ, et al. 4D PET/CT: radiology imaging to radiation therapy. Pract Radiat Oncol 2013;3:S28. https://doi.org/10.1016/j.prro.2013.01.096.
[23] Lamare F, Bousse A, Thielemans K, Liu C, Merlin T, Fayad H, et al. PET respiratory motion correction: quo vadis? Phys Med Biol 2022;67:1–27. https://doi.org/10.1088/1361-6560/ac43fc.
[24] Kauweloa KI, Ruan D, Park JC, Sandhu A, Kim GY, Pawlicki T, et al. GateCT surface tracking system for respiratory signal reconstruction in 4DCT imaging. Med Phys 2012;39:492–502. https://doi.org/10.1118/1.3671941.
[25] Liu HH, Balter P, Tutt T, Choi B, Zhang J, Wang C, et al. Assessing respiration-induced tumor motion and internal target volume using four-dimensional computed tomography for radiotherapy of lung cancer. Int J Radiat Oncol Biol Phys 2007;68:531–40. https://doi.org/10.1016/j.ijrobp.2006.12.066.
[26] Bettinardi V, Picchio M, Di Muzio N, Gilardi MC. Motion management in positron emission tomography/computed tomography for radiation treatment planning. Semin Nucl Med 2012;42:289–307. https://doi.org/10.1053/j.semnuclmed.2012.04.001.
[27] Barton MB, Jacob S, Shafiq J, Wong K, Thompson SR, Hanna TP, et al. Estimating the demand for radiotherapy from the evidence: a review of changes from 2003 to 2012. Radiother Oncol 2014;112:140–4. https://doi.org/10.1016/j.radonc.2014.03.024.
[28] Feng T, Wang J, Sun Y, Zhu W, Dong Y, Li H. Self-gating: an adaptive center-of-mass approach for respiratory gating in PET. IEEE Trans Med Imaging 2018;37:1140–8. https://doi.org/10.1109/TMI.2017.2783739.
[29] Schleyer PJ, O'Doherty MJ, Barrington SF, Marsden PK. Retrospective data-driven respiratory gating for PET/CT. Phys Med Biol 2009;54:1935–50. https://doi.org/10.1088/0031-9155/54/7/005.
[30] Thielemans K, Rathore S, Engbrant F, Razifar P. Device-less gating for PET/CT using PCA. In: IEEE nuclear science symposium and medical imaging conference: Valencia, Spain; 2011. p. 3904–10. doi:10.1109/NSSMIC.2011.6153742.
[31] Pan T, Lu Y, Thomas MA, Liao Z, Luo D. New data-driven gated PET/CT free of misregistration artifacts. Int J Radiat Oncol Biol Phys 2021;109:1638–46. https://doi.org/10.1016/j.ijrobp.2020.11.014.
[32] Wang J, Bermudez D, Chen W, Durgavarjhula D, Randell C, Uyanik M, et al. Motion correction strategies for enhancing whole-body PET imaging. Front Nucl Med 2024. https://doi.org/10.3389/fnume.2024.1257880.
[33] Townsend DW, Geissbuhler A, Defrise M, Hoffman EJ, Spinks TJ, Bailey DL, et al. Fully three-dimensional reconstruction for a PET camera with retractable septa. IEEE Trans Med Imaging 1991;10:505–12. https://doi.org/10.1109/42.108584.
[34] Surti S. Update on time-of-flight PET imaging. J Nucl Med 2015;56:98–105. https://doi.org/10.2967/jnumed.114.145029.
[35] Schaart DR, van Dam HT, Seifert S, Vinke R, Dendooven P, Lohner H, et al. A novel, SiPM-array-based, monolithic scintillator detector for PET. Phys Med Biol 2009;54:3501–12. https://doi.org/10.1088/0031-9155/54/11/015.
[36] Prenosil GA, Sari H, Furstner M, Afshar-Oromieh A, Shi K, Rominger A, et al. Performance characteristics of the biograph vision quadra PET/CT system with a long axial field of view using the NEMA NU 2–2018 standard. J Nucl Med 2022;63:476–84. https://doi.org/10.2967/jnumed.121.261972.
[37] Ng QK, Triumbari EKA, Omidvari N, Cherry SR, Badawi RD, Nardo L. Total-body PET/CT – first clinical experiences and future perspectives. Semin Nucl Med 2022;52:330–9. https://doi.org/10.1053/j.semnuclmed.2022.01.002.
[38] Pan T, Einstein SA, Kappadath SC, Grogg KS, Lois Gomez C, Alessio AM, et al. Performance evaluation of the 5-ring GE discovery MI PET/CT system using the national electrical manufacturers association NU 2–2012 standard. Med Phys 2019;46:3025–33. https://doi.org/10.1002/mp.13576.
[39] Kesner AL, Kuntner C. A new fast and fully automated software based algorithm for extracting respiratory signal from raw PET data and its comparison to other methods. Med Phys 2010;37:5550–9. https://doi.org/10.1118/1.3483784.
[40] Yang J, Khalighi M, Hope TA, Ordovas K, Seo Y. Technical Note: Fast respiratory motion estimation using sorted singles without unlist processing: a feasibility study. Med Phys 2017;44:1632–7. https://doi.org/10.1002/mp.12115.
[41] Klein GJ, Reutter BW, Botvinick EH, Budinger TF, Huesman RH. Fine-scale motion detection using intrinsic list mode PET information. In: Proceedings IEEE workshop on mathematical methods in biomedical image analysis; 2001. p. 71–8. doi:10.1109/MMBIA.2001.991701.
[42] Bundschuh RA, Martinez-Moeller A, Essler M, Martinez MJ, Nekolla SG, Ziegler SI, et al. Postacquisition detection of tumor motion in the lung and upper abdomen using list-mode PET data: a feasibility study. J Nucl Med 2007;48:758–63. https://doi.org/10.2967/jnumed.106.035279.
[43] Buther F, Ernst I, Dawood M, Kraxner P, Schafers M, Schober O, et al. Detection of respiratory tumour motion using intrinsic list mode-driven gating in positron emission tomography. Eur J Nucl Med Mol Imaging 2010;37:2315–27. https://doi.org/10.1007/s00259-010-1533-y.
[44] Feng B, Bruyant PP, Pretorius PH, Beach RD, Gifford HC, Dey J, et al. Estimation of the rigid-body motion from three-dimensional images using a generalized center-of-mass points approach. IEEE Trans Nucl Sci 2006;53:2712–8. https://doi.org/10.1109/TNS.2006.882747.
[45] Xu J, Tsui BM. Improved intrinsic motion detection using time-of-flight PET. IEEE Trans Med Imaging 2015;34:2131–45. https://doi.org/10.1109/TMI.2015.2423976.
[46] He J, O'Keefe GJ, Gong SJ, Jones G, Saunder T, Scott AM, et al. A novel method for respiratory motion gated with geometric sensitivity of the scanner in 3D PET. In: IEEE Trans. Nucl. Sci.: Dresden Germany; 2008. p. 2557–65. doi:10.1109/TNS.2008.2001187.
[47] He J, O'Keefe GJ, Jones G, Saunder T, Gong SJ, Geso M, et al. Evaluation of geometrical sensitivity for respiratory motion gating by GATE and NCAT simulation. In: 29th annual international conference of the IEEE EMBS: Lyon, France; 2007. p. 4165–68. doi:10.1109/IEMBS.2007.4353254.
[48] Ren S, Jin X, Chan C, Jian Y, Mulnix T, Liu C, et al. Data-driven event-by-event respiratory motion correction using TOF PET list-mode centroid of distribution. Phys Med Biol 2017;62:4741–55. https://doi.org/10.1088/1361-6560/aa700c.
[49] Feng T, Zhu W, Deng Z, Yang G, Sun Y, Dong Y, et al. Real-time data-driven respiratory gating with optimized automatic VOI selection. In: IEEE nuclear science symposium, medical imaging conference and room-temperature semiconductor detector workshop (NSS/MIC/RTSD); 2016. doi:10.1109/NSSMIC.2016.8069579.
[50] Visvikis D, Barret O, Fryer TD, Turzo A, Lamare F, Cheze Le Rest C, et al. A posteriori respiratory motion gating of dynamic PET images. In: IEEE nuclear science symposium and medical imaging conference: Portland, Oregon; 2003. p. 3276–80. doi:10.1109/NSSMIC.2003.1352596.
[51] Kesner AL, Bundschuh RA, Detorie NC, Dahlbom M, Ziegler SI, Czernin J, et al. Respiratory gated PET derived in a fully automated manner from raw PET data. IEEE Trans Nucl Sci 2009;56:677–86. https://doi.org/10.1109/TNS.2009.2016341.
[52] Kesner AL, Bundschuh RA, Detorie NC, Dahlbom M, Czernin J, Silverman DHS. Respiratory gated PET derived from raw PET data. IEEE Trans. Nucl. Sci. Symp.: 2686-2691; Oct 30-Nov 3, 2007, 2007; Honolulu, Hawaii. doi:10.1109/NSSMIC.2007.4436699.
[53] Buther F, Jones J, Seifert R, Stegger L, Schleyer P, Schafers M. Clinical evaluation of a data-driven respiratory gating algorithm for whole-body PET with continuous bed motion. J Nucl Med 2020;61:1520–7. https://doi.org/10.2967/jnumed.119.235770.
[54] Miyaji N, Miwa K, Yamashita K, Motegi K, Wagatsuma K, Kamitaka Y, et al. Impact of irregular waveforms on data-driven respiratory gated PET/CT images processed using MotionFree algorithm. Ann Nucl Med 2023;37:665–74. https://doi.org/10.1007/s12149-023-01870-9.
[55] Thielemans K, Schleyer P, Marsden PK, Manjeshwar RM, Wollenweber SD, Ganin A. Comparison of different methods for data-driven respiratory gating of PET data. In: IEEE nuclear science symposium and medical imaging conference; 2013. p. 1–4. doi:10.1109/NSSMIC.2013.6829055.
[56] Ren S, Lu Y, Bertolli O, Thielemans K, Carson RE. Event-by-event non-rigid data-driven PET respiratory motion correction methods: comparison of principal component analysis and centroid of distribution. Phys Med Biol 2019;64:165014. https://doi.org/10.1088/1361-6560/ab0bc9.
[57] Greenacre M, Groenen PJF, Hastie T, D'Enza AI, Markos A, Tuzhilina E. Principal component analysis. Nat Rev Methods Primers 2022;2:100. https://doi.org/10.1038/s43586-022-00184-w.
[58] Li T, Xie Z, Qi W, Asma E, Qi J. Unsupervised deep learning framework for data-driven gating in positron emission tomography. Med Phys 2023;50:6047–59. https://doi.org/10.1002/mp.16642.
[59] Bertolli O, Arridge S, Wollenweber SD, Stearns CW, Hutton BF, Thielemans K. Sign determination methods for the respiratory signal in data-driven PET gating. Phys Med Biol 2017;62:3204–20. https://doi.org/10.1088/1361-6560/aa6052.

[60] Schleyer PJ, O'Doherty MJ, Marsden PK. Extension of a data-driven gating technique to 3D, whole body PET studies. Phys Med Biol 2011;56:3953–65. https://doi.org/10.1088/0031-9155/56/13/013.
[61] Berg E, Cherry SR. Innovations in instrumentation for positron emission tomography. Semin Nucl Med 2018;48:311–31. https://doi.org/10.1053/j.semnuclmed.2018.02.006.
[62] Andersen F, Dejanovic D, Andersen P, Berthelsen A, Jeppe F, Askløf M, et al. Implementing deep inspiration breath-hold for radiation therapy on a long axial field of view scanner. J Nucl Med 2023;64:569.
[63] Kesner AL, Chung JH, Lind KE, Kwak JJ, Lynch D, Burckhardt D, et al. Validation of software gating: a practical technology for respiratory motion correction in PET. Radiology 2016;281:239–48. https://doi.org/10.1148/radiol.2016152105.
[64] Walker MD, Morgan AJ, Bradley KM, McGowan DR. Data-driven respiratory gating outperforms device-based gating for clinical (18)F-FDG PET/CT. J Nucl Med 2020;61:1678–83. https://doi.org/10.2967/jnumed.120.242248.
[65] Dias AH, Schleyer P, Vendelbo MH, Hjorthaug K, Gormsen LC, Munk OL. Clinical feasibility and impact of data-driven respiratory motion compensation studied in 200 whole-body (18)F-FDG PET/CT scans. EJNMMI Res 2022;12:16. https://doi.org/10.1186/s13550-022-00887-x.
[66] Messerli M, Liberini V, Grunig H, Maurer A, Skawran S, Lohaus N, et al. Clinical evaluation of data-driven respiratory gating for PET/CT in an oncological cohort of 149 patients: impact on image quality and patient management. Br J Radiol 2021;94:20201350. https://doi.org/10.1259/bjr.20201350.
[67] Thomas MA, Meier JG, Mawlawi OR, Sun P, Pan T. Impact of acquisition time and misregistration with CT on data-driven gated PET. Phys Med Biol 2022;67:1–17. https://doi.org/10.1088/1361-6560/ac5f73.
[68] Meier JG, Diab RH, Connor TM, Mawlawi OR. Impact of low injected activity on data driven respiratory gating for PET/CT imaging with continuous bed motion. J Appl Clin Med Phys 2022;23:e13619. https://doi.org/10.1002/acm2.13619.
[69] Sun P, Thomas MA, Luo D, Pan T. New full-counts phase-matched data-driven gated (DDG) PET/CT. Med Phys 2024;51:1–9. https://doi.org/10.1002/mp.17097.
[70] Kang SY, Moon BS, Kim HO, Yoon HJ, Kim BS. The impact of data-driven respiratory gating in clinical F-18 FDG PET/CT: comparison of free breathing and deep-expiration breath-hold CT protocol. Ann Nucl Med 2021;35:328–37. https://doi.org/10.1007/s12149-020-01574-4.
[71] Zeng R, Fessler JA, Balter JM, Balter PA. Iterative sorting for four-dimensional CT images based on internal anatomy motion. Med Phys 2008;35:917–26. https://doi.org/10.1118/1.2837286.
[72] Li R, Lewis JH, Cervĩo LI, Jiang SB. 4D CT sorting based on patient internal anatomy. Phys Med Biol 2009;54:4821–33. https://doi.org/10.1088/0031-9155/54/15/012.
[73] Hui C, Suh Y, Robertson D, Pan T, Das P, Crane CH, et al. Internal respiratory surrogate in multislice 4D CT using a combination of Fourier transform and anatomical features. Med Phys 2015;42:4338–48. https://doi.org/10.1118/1.4922692.
[74] Carnes G, Gaede S, Yu E, Van Dyk J, Battista J, Lee TY. A fully automated non-external marker 4D-CT sorting algorithm using a serial cine scanning protocol. Phys Med Biol 2009;54:2049–66. https://doi.org/10.1088/0031-9155/54/7/013.
[75] Martin R, Pan T. Target volume and artifact evaluation of a new data-driven 4D CT. Pract Radiat Oncol 2017;7:e345–54. https://doi.org/10.1016/j.prro.2017.01.014.
[76] Pan T. Comparison of helical and cine acquisitions for 4D-CT imaging with multislice CT. Med Phys 2005;32:627–34. https://doi.org/10.1118/1.1855013.
[77] Pan T, Martin RM, Luo D. New prospective 4D-CT for mitigating the effects of irregular respiratory motion. Phys Med Biol 2017;62:N350–61. https://doi.org/10.1088/1361-6560/aa7a9b.
[78] Werner R, Sentker T, Madesta F, Schwarz A, Vornehm M, Gauer T, et al. Intelligent 4D CT sequence scanning (i4DCT): First scanner prototype implementation and phantom measurements of automated breathing signal-guided 4D CT. Med Phys 2020;47:2408–12. https://doi.org/10.1002/mp.14106.
[79] Thomas MA, Pan T. Data-driven gated PET/CT: implications for lesion segmentation and quantitation. EJNMMI Phys 2021;8:1–15. https://doi.org/10.1186/s40658-021-00411-5.
[80] Werner R, Sentker T, Madesta F, Gauer T, Hofmann C. Intelligent 4D CT sequence scanning (i4DCT): concept and performance evaluation. Med Phys 2019;46:3462–74. https://doi.org/10.1002/mp.13632.
[81] Sun P, Thomas MA, Luo D, Pan T. Correcting CT misregistration in data-driven gated (DDG) PET with PET self-gating and deformable image registration. Med Phys 2024;51:1626–36. https://doi.org/10.1002/mp.16958.
[82] Cook EL, Su K-H, Higgins GS, Johnsen R, Bouhnik J-P, McGowan DR. Data-driven gating (DDG)-based motion match for improved CTAC registration. EJNMMI Phys 2024;11:42. https://doi.org/10.1186/s40658-024-00644-0.
[83] Fayad HJ, Lamare F, Le Rest CC, Bettinardi V, Visvikis D. Generation of 4-dimensional CT images based on 4-dimensional PET-derived motion fields. J Nucl Med 2013;54:631–8. https://doi.org/10.2967/jnumed.112.110809.
[84] Hamill JJ, Panin VY. TOF-MLAA for attenuation correction in thoracic PET/CT. In: IEEE nuclear science symposium and medical imaging conference: Anaheim, California; 2012. p. 4040–47. doi:10.1109/NSSMIC.2012.6551924.
[85] Lu Y, Fontaine K, Mulnix T, Onofrey JA, Ren S, Panin V, et al. Respiratory motion compensation for PET/CT with motion information derived from matched attenuation-corrected gated PET data. J Nucl Med 2018;59:1480–6. https://doi.org/10.2967/jnumed.117.203000.
[86] Rezaei A, Defrise M, Bal G, Michel C, Conti M, Watson C, et al. Simultaneous reconstruction of activity and attenuation in time-of-flight PET. IEEE Trans Med Imaging 2012;31:2224–33. https://doi.org/10.1109/TMI.2012.2212719.
[87] Hwang D, Kang SK, Kim KY, Choi H, Seo S, Lee JS. Data-driven respiratory phase-matched PET attenuation correction without CT. Phys Med Biol 2021:66. https://doi.org/10.1088/1361-6560/abfc8f.